Full Ion Velocity Distribution Function measurement in an Electric Thruster, using LIF-based tomographic reconstruction

IEPC-2015-235／ISTS-2015-b-235

Presented at Joint Conference of 30th International Symposium on Space Technology and Science 34th International Electric Propulsion Conference and 6th Nano-satellite Symposium, Hyogo-Kobe, Japan July 4 – 10, 2015

P.-Q. Elias[1], J. Jarrige[2], E. Cucchetti[3] and D. Packan[4]
Onera – The French Aerospace Lab, Palaiseau, F-91761, France

A. Bulit[5]
ESA ESTEC, Noordwijk, 2200 AG, The Netherlands

Abstract: Measuring the full ion velocity distribution function by non-intrusive techniques can improve our understanding of the ionization processes and beam dynamics at work in ion thrusters. In this paper, a LIF-based tomographic reconstruction technique is applied to the measurement of the IVDF in the plume of a miniature Hall Effect Thruster. A setup is developed to rotate the laser axis around the measurement volume. The LIF measurements taken from different viewing angles are combined using a filtered back-projection algorithm combined to reconstruct the IVDF. First, the setup is used to probe the most probable ion velocity in the thruster channel. Then the 2D tomographic technique is applied at two locations in the near field plume of the thruster. The results obtained in front of the thruster nose cone show that the 2D IVDF is toroidal in the phase space. The next step of this work is to perform a reconstruction of the complete (3D in phase space) IVDF.

Nomenclature

θ	[rad]	Laser angle
φ	[rad]	Laser angle
e_x, e_y, e_z	[1]	Unit vectors
e_r, e_φ	[1]	Unit vectors (laser coordinate)
λ_0	[nm]	Transition wavelength
λ_L	[nm]	Laser wavelength
ν_L	[MHz]	Laser frequency
$\delta\nu$	[MHz]	Frequency shift
V	[km/s]	Ion velocity
V_+, V_-	[km/s]	Most probable velocity
F	$[m^{-3}.s^3]$	Ion velocity distribution function
$F_{V_{z0}}$	$[m^{-2}.s^2]$	Projected ion velocity distribution function

[1] Research Scientist, Physics and Instrumentation Department, paul-quentin.elias@onera.fr
[2] Research Scientist, Physics and Instrumentation Department, julien.jarrige@onera.fr
[3] Graduate student, Physics and Instrumentation Department
[4] Research Scientist, Physics and Instrumentation Department, denis.packan@onera.fr
[5] Electric Propulsion Engineer, TEC-MPE, alexandra.bulit@esa.int

f	$[m^{-1}.s]$	Projected ion velocity distribution function
f_{Acq}	[Hz]	Acquisistion frequency
S	[a.u]	LIF signal
n_1	$[m^{-3}]$	Metastable number density
p_i	[1]	Normalized hyperfine line strength
LIF	-	Laser Induced Fluorescence
IVDF	-	Ion Velocity distribution function
FBP	-	Filtered Back Projection
FSR	-	Free Spectral Range

I. Introduction

THE optimization and the development of electric thrusters benefit from finer and improved non-intrusive measurements of the physical properties of the plasma. Among these diagnostics, Laser Induced Fluorescence has been shown to provide a wealth of information, and has been successfully applied on many thruster technologies: HET[1–4], FEEP[5]. However, “standard” LIF, as applied most of the time on thrusters, has limitations because it leads to only a partial appreciation of the ion velocity field. Indeed it can be shown that with a fixed laser beam orientation, only a projection of the ion velocity distribution is measured. Therefore such a use of LIF cannot describe complex situations in thruster plumes, such as crossing beams. Having a technique able to retrieve the full IVDF might give a new picture of current thruster physics. The main purpose of this work is thus to develop a new LIF setup and scheme to explore and reveal the full extent of the content of thrusters plumes. The method proposed is based on LIF tomography in phase space. This technique has been pioneered by McWilliams and Koslover[6 7], to study a Barium plasma simulating ionospheric processes. These measurements were limited to a two dimensional reconstruction of the ion velocity distribution function. LIF tomography has also been used by Biloiu et al. to measure the 2D ion velocity distribution function in an argon Helicon source. This work seeks to extend this technique for Xenon-based electric thruster. The goal is to measure the full xenon ion velocity distribution function, using a three dimensional reconstruction in the velocity phase space.

The paper presents the experimental set-up specifically developed for this purpose, and detail the measurement process developed in this frame. A SPASE GmbH Hall Effect Thruster (SPT20) is used for this investigation. Examples of measurements in the thruster plume and reconstruction of the ion velocity distribution function will be presented.

II. LIF Tomography

This section presents the theory of the tomographic method applied to LIF measurements. First, a few definitions are recalled, and then the 2D reconstruction method is presented. Its extension to reconstruct the full IVDF (3D in the phase space) is finally explained.

A. LIF scheme

LIF diagnostics on Xenon ions has mainly used two popular transitions: 605.1 nm and 834.7 nm. These transitions are shown in the partial Gotrian chart in Figure 1. In principle, other schemes can be used [3]. In this study, the ionic transition probed is the one at 834.7 nm. The 605.1 nm transition, while well-known theoretically, can only be probed with dye Lasers. For the measurement planned in this study, the use of such a laser is too impractical, in particular due to their limitation in the tuning range for a given mixture of dyes (typically ~10 GHz). The transition at 834.7 nm is less known theoretically, but it can be probed by tunable laser diodes, which are much more compact, have larger tunable range (~typically 20-30 GHz mode-hop free ranges).

The 834.7 nm LIF scheme used for Xenon ions is a multi-level scheme. This means that it starts from a metastable state (not the ground state). The laser pumps the ion to an excited state, and the fluorescence signal results from the decay of this excited state to a third state. The different electronic levels involved in this scheme are shown in Table 1.

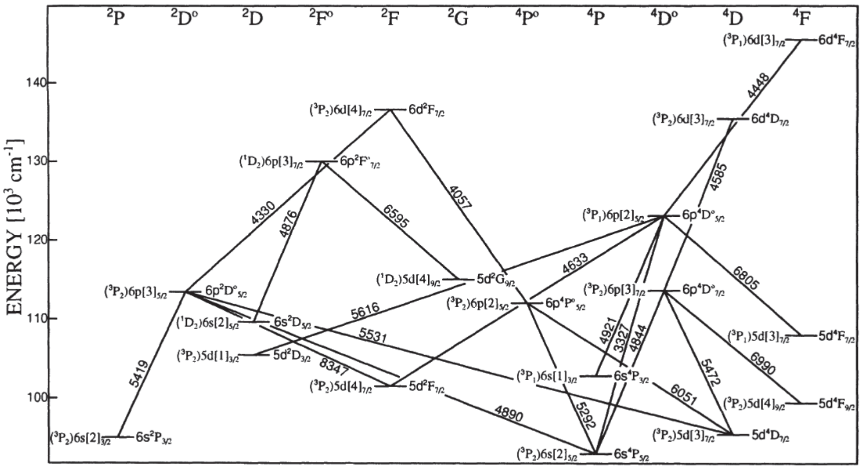

Figure 1-Partial Gotrian diagram of Xe II, from [4]

The vacuum wavelength of the probed transition is 834.9565 nm (wavelength in air 834.7313).

Table 1 - Electronic levels of the 834.7 nm LIF scheme

	Configuration	Level	L	S	J	g_J	Energy (eV)
Probed Level (Lower level)	5p^4 ($^3P_2$) 5d	5d $^2F_{7/2}$	3	½	7/2	1.143188	12.588818
Pumped Level (Higher level)	5p^4 ($^3P_2$) 6p	6p $^2D^0_{5/2}$	2	½	5/2	1.200464	14.073738
Decay Level	5p^4 ($^3P_2$) 6s	6s $^2P_{3/2}$	1	½	3/2		11.786480

B. Definitions

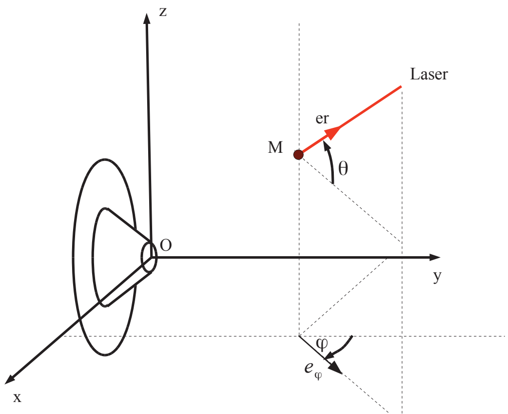

Figure 2- coordinate system for the tomographic reconstruction

The thruster coordinate system has its origin O at the tip of the central cone of the SPT20 thruster. The y axis is the axis of the thruster. The measurement point is defined by its coordinates (x,y,z). An ion velocity vector at the measurement point M is given by:

$$\vec{V} = V_x\vec{e_x} + V_y\vec{e}_y + V_z\vec{e}_z \qquad (II.1)$$

At the measurement point M, the ion velocity distribution function is given as function of V_x, V_z and V_z:

$$F(V_x, V_y, V_z) \qquad (II.2)$$

The laser beam orientation is given by two angles, θ and(II.3) φ, as shown in Figure 2. The laser beam axis is given by the vector $\vec{e}_r$, defined as:

$$\vec{e}_r = \sin(\varphi)\cos(\theta)\,\vec{e}_x + \cos(\varphi)\cos(\theta)\,\vec{e}_y + \sin(\theta)\vec{e}_z \quad (II.4)$$

When the laser frequency is ν_L, and assuming that the transition frequency is ν_0, the velocity class sampled by the laser has its projected velocity along the laser axis given by:

$$\vec{V}.\vec{e}_r = V(\nu_L) = -\lambda_0(\nu_L - \nu_0) \quad (II.5)$$

If the laser frequency is above transition frequency, this means that the probed population moves away from the laser.

For a given laser orientation and a given laser frequency ν_L, we can define the projected ion velocity distribution function which include the contribution of all the population having a velocity such as eq. (II.5) is true (this equation defines a plane in the phase space). This means in particular that the projected ion velocity distribution function must include that contribution of F with the velocity in the plane of the phase space defined as

$$V(\nu_L) - \sin(\varphi)\cos(\theta)\,V_x - \cos(\varphi)\cos(\theta)V_y - \sin(\theta)\,V_z = 0 \quad (II.6)$$

The projected ion velocity distribution function, for a given laser orientation (φ, θ) is given by:

$$f(V) = \int dV_x dV_y dV_z F(V_x, V_y, V_z)\delta(V - \sin(\varphi)\cos(\theta)\,V_x - \cos(\varphi)\cos(\theta)V_y - \sin(\theta)\,V_z) \quad (II.7)$$

Where V is the velocity given in (II.5).

C. Results of a LIF measurements

As recalled in section A, the transition used for the LIF measurements on the Xenon ions has a hyperfine structure. This means that the laser do not probe a single line, but several lines. Let us assume that the transition has N lines of relative intensity p_i. Then, assuming that the laser intensity is slow enough to be in the linear regime, the LIF signal collected by the detection is given by:

$$S(\nu_L) = \alpha\, n_1 \sum_{i=1}^{N} p_i f\big(\lambda_0(\nu_L - \nu_{0i})\big) \quad (II.8)$$

Where α is a constant that includes the Einstein coefficient of the transition, the measurement volume and its viewing factor. The quantity of interest in this equation is f, the projected ion velocity distribution. Normally, retrieving this function requires a deconvolution of the signal S. This is illustrated in the Figure 3, showing the reference LIF signal obtained in the reference discharge cell. The LIF signal width is of the order of 1 GHz, while the main lines of the hyperfine structure are roughly spread over 500 MHz. In this case, it is necessary to account for this spread by using a deconvolution, as done in [8]. However, if the width of the LIF signal is much larger than the spread of the lines of the transition, then the LIF signal can be taken directly as the projected velocity distribution function. This is the case for the LIF signal measured in the SPT20 thruster, as shown in Figure 4. In this example, the narrowest LIF signal measured in the thruster channel is considered. The width at half maximum of the LIF spectrum is about 3.1 GHz, much broader than the reference signal and also the spread of the hyperfine lines. In this condition, it is safe to consider that the measured LIF spectrum is proportional to the projected velocity distribution function f. This assumption is also found in the literature [9].

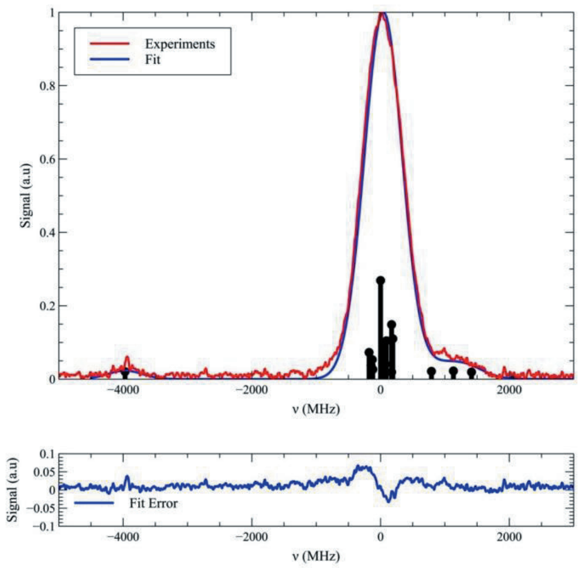

Figure 3- Reference LIF signal, and the fitted value obtain from the hyperfine lines (black) convolved with a gaussian function

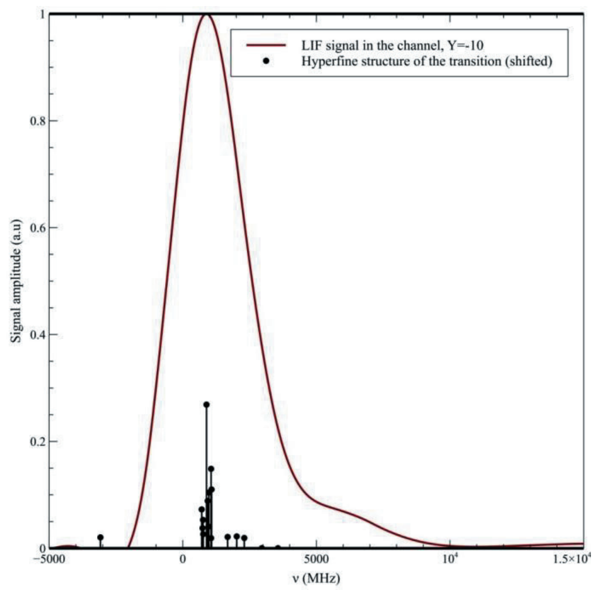

Figure 4- LIF signal inside the SPT20 channel shown with the shifted lines (black) of the transition.

D. 2D Tomographic reconstruction

For simplicity, let us assume that $\varphi = 0$, and that only θ can vary. This situation is shown in Figure 5. Following the expression (II.7) that gives the projected velocity function, the LIF measurements yields the following projected velocity distribution function

$$f_\theta(V) = \int dV_x dV_y dV_z F\left(V_x, V_y, V_z\right) \delta(V - \cos(\theta) V_y - \sin(\theta)\, V_z) \tag{II.9}$$

Let us define f_2 the 2-dimensional ion velocity distribution function obtained by projection on the plan Vy-Vz.

$$f_2(V_y, V_z) = \int_{-\infty}^{\infty} f(V_x, V_z, V_z) dV_x \qquad (II.10)$$

Then equation (II.9) can be written as:

$$f_\theta(V) = \int dV_y dV_z f_2(V_y, V_z) \delta(V - \cos(\theta) V_y - \sin(\theta) V_z) \qquad (II.11)$$

This expression corresponds to the definition of the Radon transform [10] noted $Rf(\theta, V)$. Therefore, if the viewing angle θ is varied, it is possible to obtain a sinogram of the projected IVDF f_2. The whole formalism of tomographic reconstruction can then be applied to the sinogram. From the sinogram, the filtered back projection algorithm [10] can be used to reconstruct f_2. Figure 6, Figure 7 and Figure 8 show examples of the reconstruction when the number of viewing angles is changed.

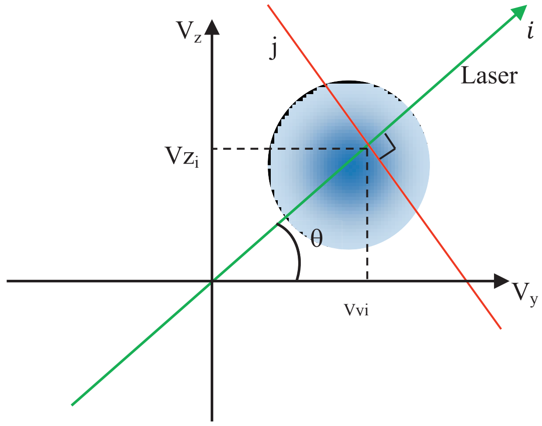

Figure 5 - ion velocity distribution function measurements for φ=0

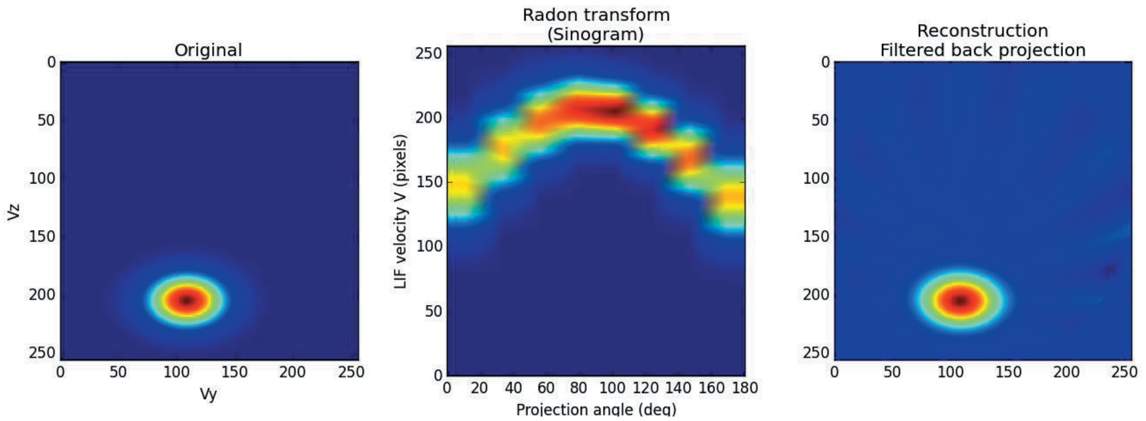

Figure 6- Examples of a tomographic reconstruction with the FBP algorithm (8 viewing angles between 0-180°)

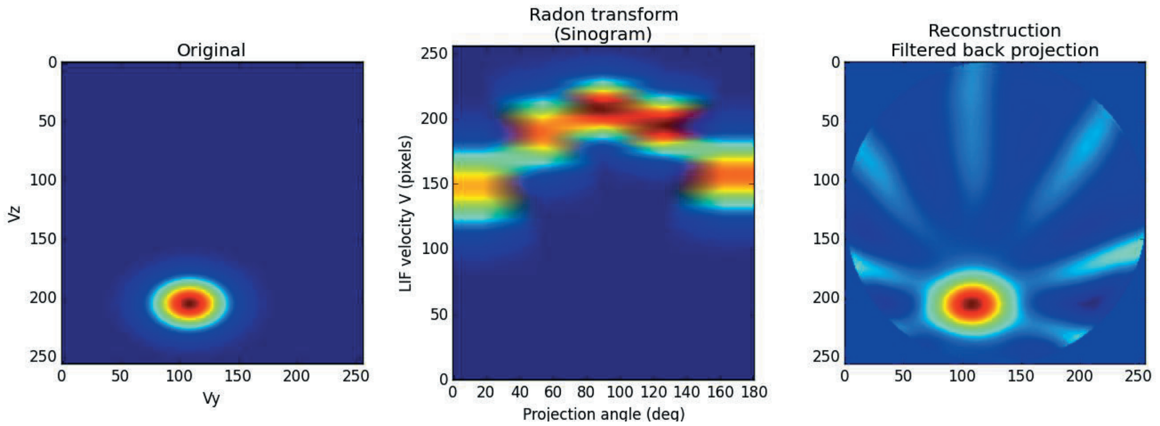

Figure 7 - Examples of a tomographic reconstruction with the FBP algorithm (5 viewing angles between 0-180°)

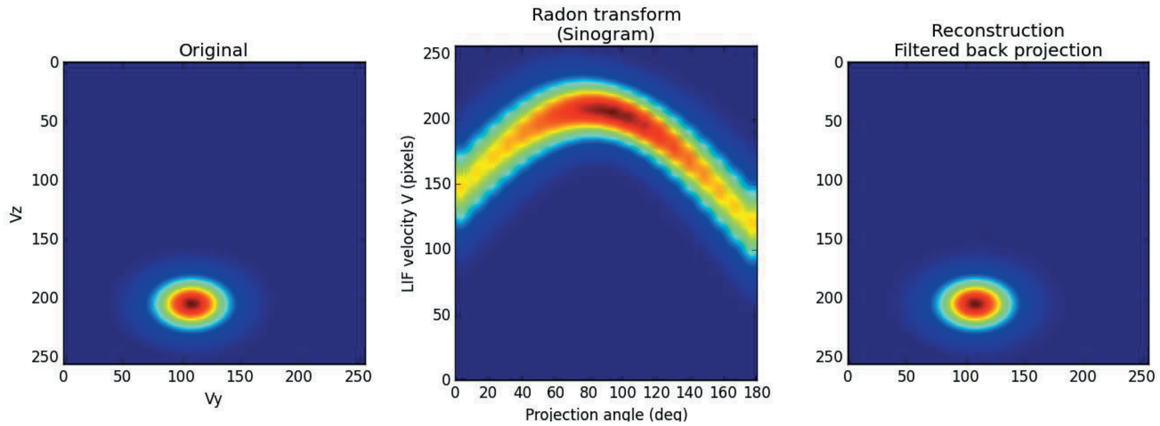

Figure 8- Examples of a tomographic reconstruction with the FBP algorithm (20 viewing angles between 0-180°)

If φ is different from zero, then FBP algorithm retrieve the IVDF projected on a plane defined by the vectors $(\boldsymbol{e}_{\boldsymbol{\varphi}}, \boldsymbol{e}_{\boldsymbol{z}})$. Therefore, if we note V_φ the velocity along the vector e_φ, then reconstruction algorithm gives $f_2(V_\varphi, V_z)$.

E. 3D reconstruction

Let us assume that the 2D reconstruction described above is repeated for several angles φ. This process yields a set of projected 2D IVDF $f_2(V_\varphi, V_z)$. From this set of equations, let us consider the restrictions such as $V_z = V_{z0}$. The function $F_{V_{z0}}(V_\varphi) = f_2(V_\varphi, V_{z0})$ is the projection along the plane $(\boldsymbol{e}_{\boldsymbol{\varphi}}, \boldsymbol{e}_{\boldsymbol{z}})$ of the velocity distribution function of ions having a velocity along z given by $V_z = V_{z0}$. Therefore, for this class of ions, seen form multiple viewing angles φ, the FBP algorithm can reconstruct the 2-dimensional IVDF along V_x and V_y of the ions having a velocity V_{z0} along the z axis. When the process is repeated for all the velocities along the z-axis, a full 3-dimensional reconstruction of the IVDF is obtained.

To summarize, the whole process is illustrated in the Figure 9 below.

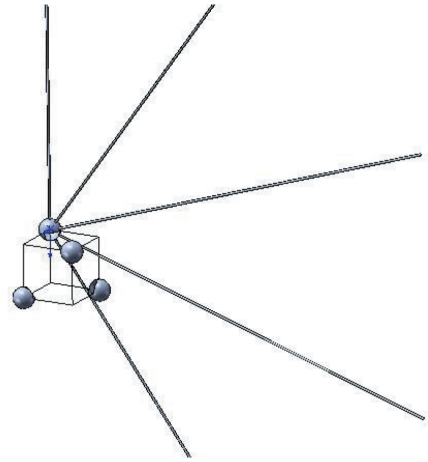

a) Initial IVDF (4 gaussian-shaped distributions)

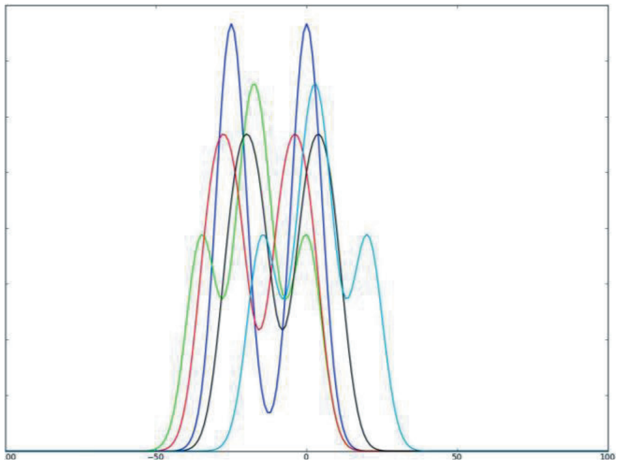

b) LIF signal for a given φ and 5 different θ

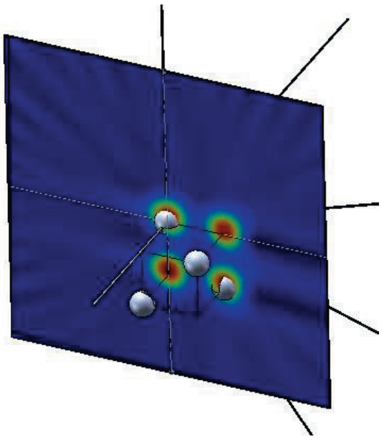

c) 2D reconstruction for a given φ

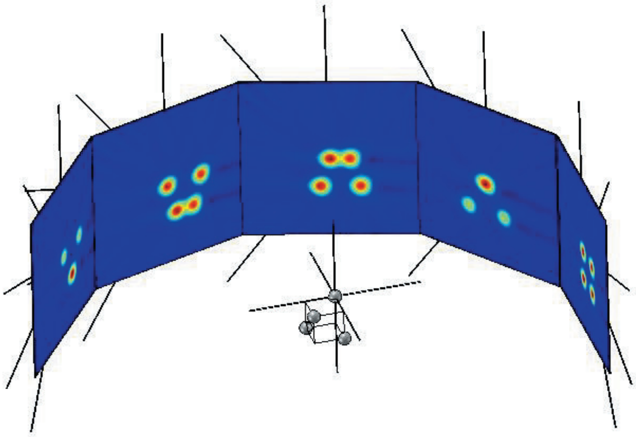

d) Set of 2D IVDF for different φ

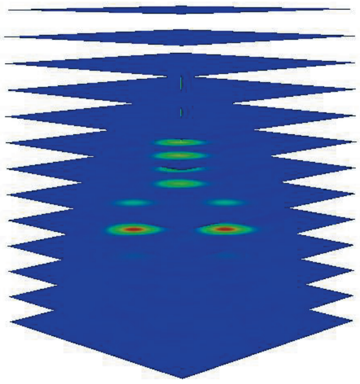

e) 3D IVDF obtained from the set of 2D IVDFs

Figure 9 – LIF tomography reconstruction method

III. Experimental Setup

F. Optical setup

A schematic of the optical setup used in this study is shown in Figure 10. The laser is a SDL-TC10 tunable laser diode. Its typical output power is 20 mW and its maximum fine tuning range is 60 GHz (typical 40 GHz - 700 eV in Xe). Its frequency jitter is less than 2 MHz, and the light polarization is TE (horizontal wrt to the diode assembly). A LM007 Lambdameter measures the laser wavelength. This device uses 4 temperature–stabilized Fizeau interferometers to measure the wavelength with a relative accuracy of 10^{-7}, and an absolute accuracy of 60 MHz.

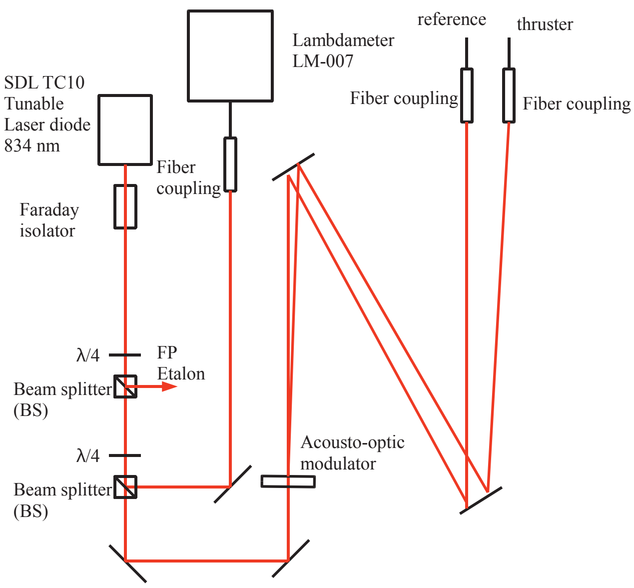

Figure 10- Optical setup schematic

G. Vacuum setup

The optical setup to perform the LIF tomography must meet the following requirements:

- Position the laser beam and the detection optic in the thruster plume to get a LIF measurement
- Rotate the optical train around the measurement volume
  - The laser beam must cover the ranges $0° \leq \theta \leq 180°$ and $0° \leq \varphi \leq 180°$ (see Figure 2)
  - Angular repeatability better than 1°
  - Angular resolution better than 1°
- Maintain the optics alignment
- The probed volume must be on the order of one cubic millimeter
- The probed volume must not deviate of more than 0.1 mm while rotating the optical train
- The laser beam and detection optical angle must be kept constant

In additions to these specifications, the setup must be computer controlled, and capable to perform alignment operations while in vacuum. The solution developed to meet these requirements is composed of three main components:

- A rotation stage (vertical rotation, angle φ)
- A circular translation stage (horizontal rotation, angle θ)
- A carriage, holding the optics on the circular translation stage

Figure 11 shows the whole setup, including the 3-axis translation stage that holds the thruster. The width of the arch has been minimized to reduce its influence on the plume. The components most sensitive to sputtering (motor, gear, rail and wheels, sensors) are kept out of direct impact from the plume. The horizontal rotation (angle θ) is enabled by a circular translation stage. It is composed of a circular precision stainless-steel rail, a geared circular beam, and a protective aluminum cover. This assembly is hereafter referred to as the arch or circular translation stage. This circular translation stage covers a circle portion of 240°. The inner diameter is 440 mm, the outer is 580 mm. It is machined with tight tolerance, (parallelism 0.013 mm/m, straightness 0.2 mm/m) to guide the carriages. A stainless steel geared circular beam is used for the worm drive moving the carriages. Finally a protective cover is used to protect the cables, the gears, the encoders and the optics.

The table below summarizes the actual setup performances, based on the technical implementation presented in this document.

Table 2 - Summary of the setup performances

Setup weight	8 kg
Inner diameter of the circular translation stage	440 mm
Outer diameter	580 mm
Angular resolution on φ	0.001°
Angular repeatability on φ	0.005°
Angular resolution on θ	0.001°
Angular repeatability on θ	0.005°
Swept angle φ	270°
Swept angle θ	210°
Measurement point volume	1.2 mm diameter sphere
Measurement point spatial jitter	< 80 µm

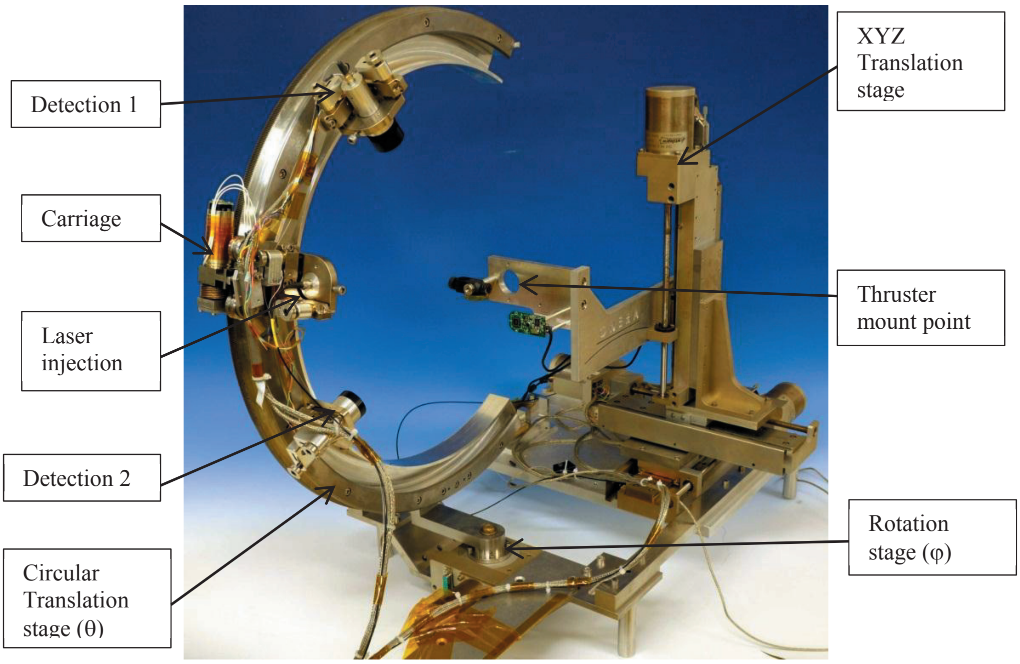

Figure 11- Main view of the experimental setup

H. SPT20 Thruster
For this work, a SPASE GmbH SPT20 thruster is used as the device under test. Its operation ranges are summarized in Table 4 below. The thruster and the vacuum setup presented above are installed in Onera B09 vacuum tank. The characteristics of this facility are given in Table 3 below:

Table 3- B09 vacuum chamber characteristics

Diameter	800 mm
Length	2000 mm

Measured Pumping speed for Xenon :	2050 L/s
Measured Chamber ultimate pressure:	< 4.10^{-7} mbar (for Air)
Measured Chamber pressure for m=0.4 mg/s Xe	1.6.10^{-5} mbar (for Air)
Xenon Pressure for m=0.4 mg/s Xe	6.4.10^{-6} mbar Xe

Table 4- Spase GmbH SPT20 parameters

Parameter	min	nominal	max
Ultimate Vacuum pressure, mbar	10^{-6}	10^{-7}	
Discharge voltage, V	150	300	320
Discharge current, mA		0.3	0.4
Discharge power, W		90	120
Coil current	1.5	2.5	3.5
Anode mass flow rate, mg/s (Xe)	0.28	0.31	0.35
Cathode flow rate, mg/s (Xe)		0.1	

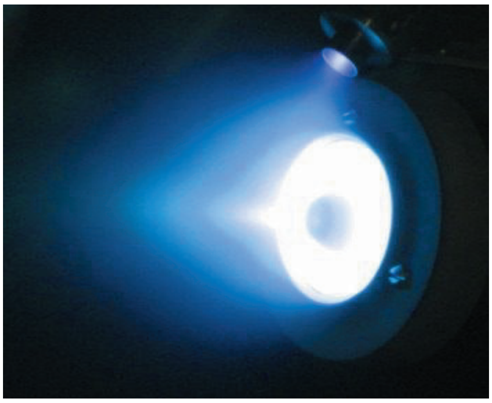

Figure 12- View of the SPT20M in Onera B09 vacuum tank

I. Wavelength calibration

A reference discharge (surfatron discharge in Xe) provides the zero-velocity reference for the LIF transition[2]. The laser wavelength is measured by counting the transmission peaks on the Fabry-Perot Etalon. The Fabry Perot is a 230 mm long cavity whose free spectral range (FSR), given by the frequency range between two successive peaks, is determined with the following procedure:

- The laser frequency is swept using an triangle signal
- A synchronous acquisition of the Lambda Meter and the Photodiode of the Fabry-Perot etalon is recorded
- The timing of the different peaks on the Fabry Perot signal are detected using a peak detection algorithm
- The laser wavelength at each peak is recorded
- The peak frequency versus the peak number is plotted; the slope gives the FSR.

In Figure 13 an example of the peak detection algorithm is given. In Figure 14, the Frequency-Peak Index curves for an increasing and decreasing sweep is given. Considering the relative and absolute uncertainty of the Lambda Meter, and the uncertainty in the peak detection method, the FSR computed from this method is:

$$FSR = 640 \pm 0.35\ MHz \qquad \text{(III.1)}$$

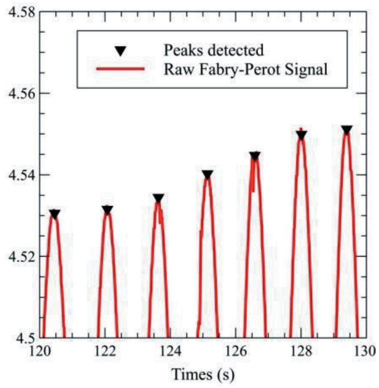

Figure 13- Peak detection on the Fabry-Perot signal

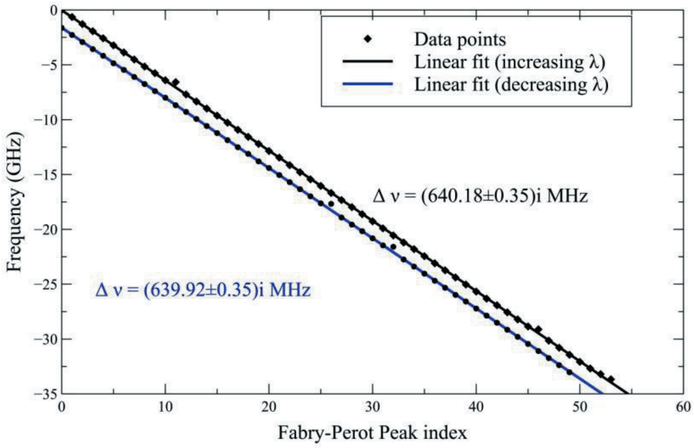

Figure 14- Frequency vs FP peak index

The zero of the wavelength axis is defined relative to the reference discharge LIF signal. The peak of the reference LIF signal gives the position of the transition. Since all wavelengths are defined relative to this reference, the uncertainty in the wavelength arises only from the Fabry-Perot. To calibrate the frequency axis, the time evolution of the Fabry-Perot signal is recorded. The FSR, ie the frequency shift between the successive peaks is known (with uncertainty). The calibration implies to detect each peak and the time of its occurrence.

$$\nu(t) = \frac{FSR}{\Delta t}(t - t_0) + n\,FSR \tag{III.2}$$

$$\delta\nu \leq \sqrt{(n+1)\delta FSR^2 + 3FSR^2\frac{\delta t^2}{\Delta t^2}} \tag{III.3}$$

Here δFSR is the uncertainty in the measurement of the Fabry-Perot FSR, δt is the uncertainty in the peak timing detection. The uncertainty on the laser frequency can be estimated when we consider that a given scan has typically a width enough to detect 300 eV Xenon ions. This requires a bandwidth of 24 GHz, in which we can count 38 FSR of the Fabry-Perot etalon. Thus, with $n = 38$, $\delta t = 10/f_{acq}$ (the uncertainty on the peak detection is a few sampling intervals), and a scan speed of $S = 50\ MHz/s$, giving $\Delta t = FSR/S$, we get the following estimate for the laser frequency

$$\delta\nu \leq 12\ MHz$$

IV. Results

J. Thruster axial velocity

First, the thruster macroscopic velocity in the thruster channel is investigated. The thruster is operated with the following conditions: Discharge voltage U_d=300 V, discharge current $I_d = 380\ mA$, Anode mass flow rate $\dot{m}_a = 0.31\ mg/s$, coil current $I_c = 2.14\ A$. The background pressure during the measurement is $p = 4.6 \times 10^{-5}\ mbar$ in Nitrogen.

The SPT20M channel is 4 mm wide, with a mean diameter of 20 mm. The measurement axis is parallel to the thruster axis, in the center of the channel, as shown in Figure 15. The origin y=0 of the axis is defined at the thruster nose cone. The anode is located at y=-16 mm (not shown in the figure).

The velocity measurement at each location is obtained by taking two LIF measurements, with the laser angles $\theta = +22.5°$ and $\theta = -22.5°$. This tilt ensures an optimal optical access inside the thruster channel. Besides, the two measurements can be used to compute the 2D macroscopic velocity vector (see. [5] for examples).

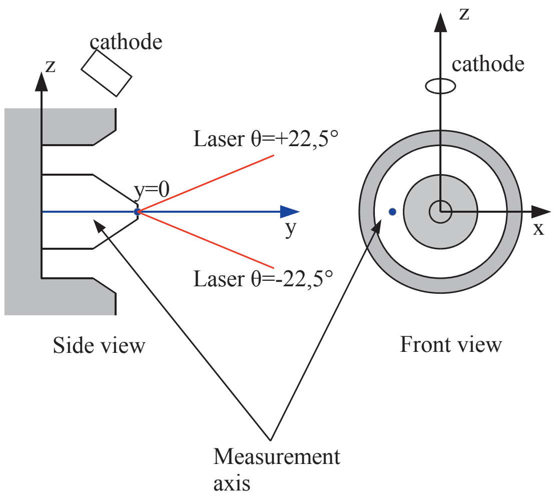

Figure 15 – Position of the measurements in the SPT20

Figure 16 shows several normalized LIF signal obtained in the thruster channel (y<0) and in the plume, up to 30 mm from the nose cone. The same data are plotted in color contours in Figure 17. These figures show that the most probable ion velocity increases sharply between y=-6 mm and y=+2 mm. For y> 2 mm , in the near field region of the thruster, the ion velocity increases slightly, from 13 km/s to 17 km/s. A population of slow ions can also be seen in this region, up to y=+25 mm. Note that these data corresponds to the case where θ=+22.5°. The measurements with θ=-22.5° exhibits the same behavior.

If we note V_+ and V_- the most probable ion velocities for $\theta = +22.5°$ and $\theta = -22.5°$, respectively, the components of the velocity in the thruster coordinate systems can be obtained:

$$V_y = \frac{V_+ + V_-}{2\cos(\theta)}$$
$$V_z = \frac{V_+ - V_-}{2\sin(\theta)} \qquad \text{(IV.1)}$$

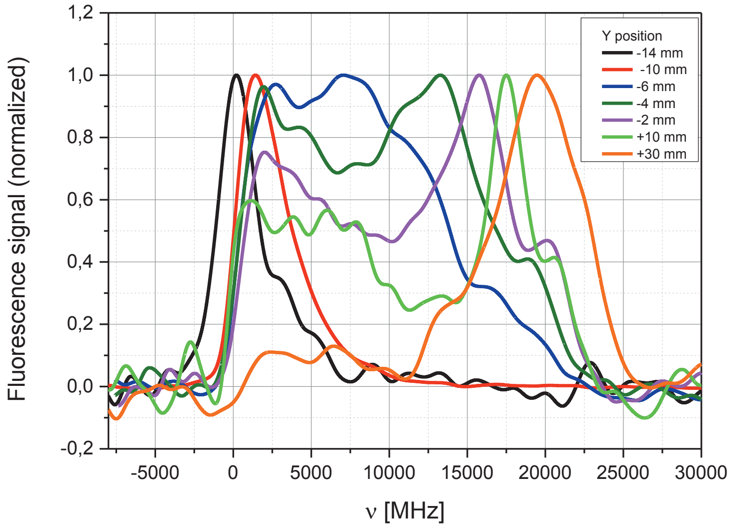

Figure 16- Normalized LIF signal obtained for different y position, laser angle θ=22.5°

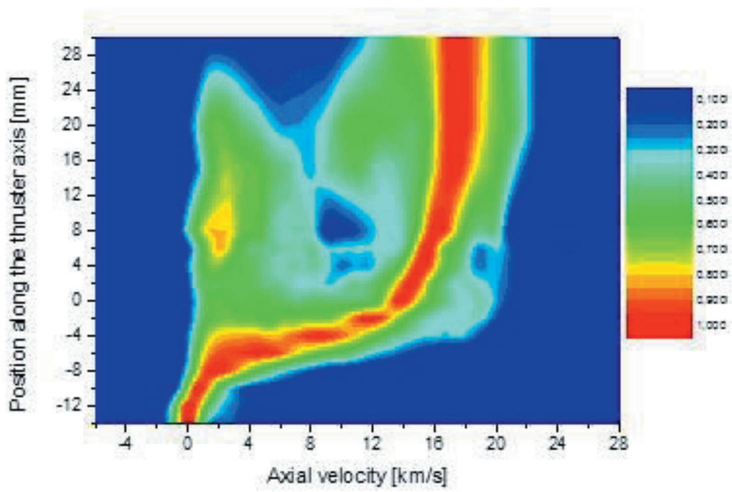

Figure 17 - Normalized LIF signal velocity map, θ=22.5°

In Figure 18, the 2 components V_y (axial) and V_z are plotted along the measurement axis. In the near field region, for y>0, the velocity vector is mainly axial, with a negligible z component. Inside the channel, for y<0, a significant V_z is measured. This component is positive, meaning that the ions drift towards the cathode (see Figure 15). Spot checks at other locations (same y position) in the channel show the same trend. This drift is likely due to the electric field distortion induced by the cathode. Such a trend has already been observed on higher-power SPT thruster [11].

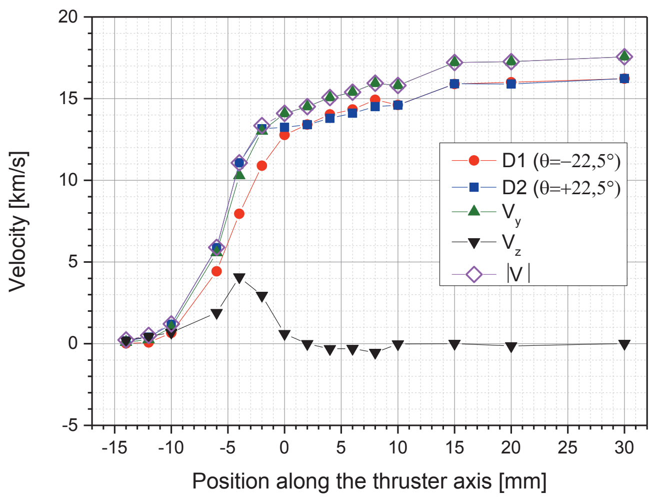

Figure 18 - Most probable ion velocities along the measurement axis

K. 2D tomographic reconstruction

For the same thruster conditions than those used for the axial LIF measurements, a 2D reconstruction of the IVDF is performed in the near field region of the thruster. The two locations used for this measurement are shown in Figure 19. Case A measures the IVDF in front of the thruster nose cone, where a narrow plasma plume can be seen. Case B considers the IVDF at the end of the acceleration region (y=+6 mm), where two populations of slow and fast ions coexist, as seen in Figure 17.

For each location, a set of 20 LIF scans are performed, covering 180°. The measurements at $\varphi = -90°$ and $\varphi = +90°$ are redundant, and are used to check the drift of the thruster and the repeatability of the signal.

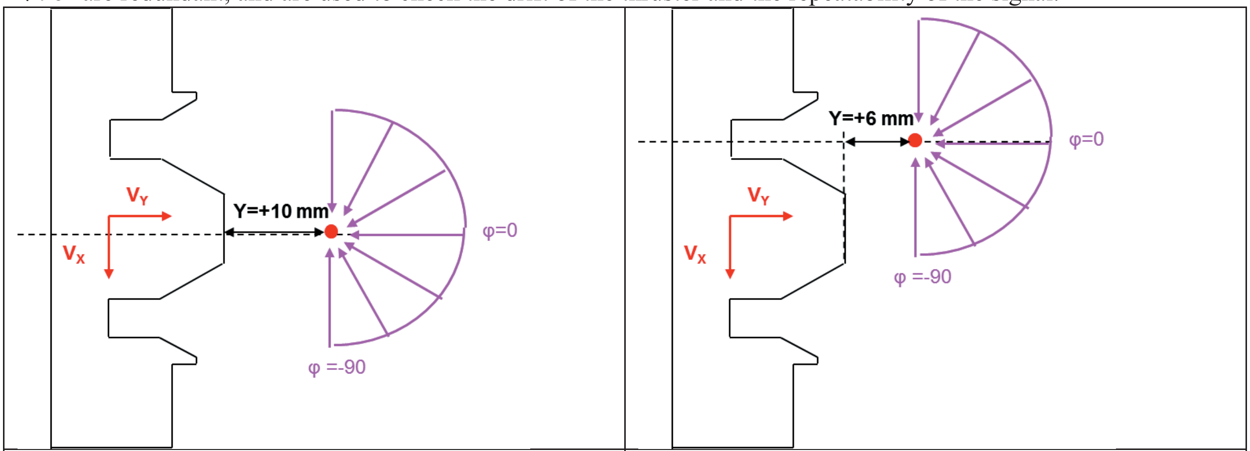

a) Case A	b) Cas B

Figure 19- Location of the 2D tomographic measurements (top cross section)

In Figure 20, examples of the LIF signals obtained in case B are shown. These data are used to retrieve the projected 2D-IVDF, as shown in Figure 21 and Figure 22.

In case A (Figure 22), two crossing ions beams can be seen. The most probable velocity of the upper beam makes a 23° angle with the thruster axis. The lower beam is less intense, but roughly symmetrical in terms of velocity magnitude and angle. This shape is not surprising since at location A, ions coming from the annular channel converges. We expect here the IVDF to have a toroidal shape.

In case B, the two populations already detected in the axial measurements are clearly separated. The slow ion population drifts slowly towards the thruster axis (magnitude of the most probable velocity ~ 3.4 km/s, angle 30°), while the fast population has a most probable velocity of 16.4 km/s, which is close to the axial velocity measured in the axial scan, as shown in Figure 18.

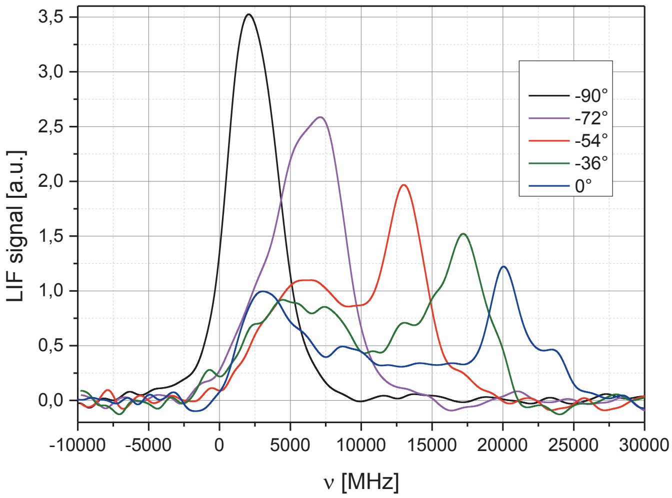

Figure 20 - Examples of the LIF signals obtained in the case B

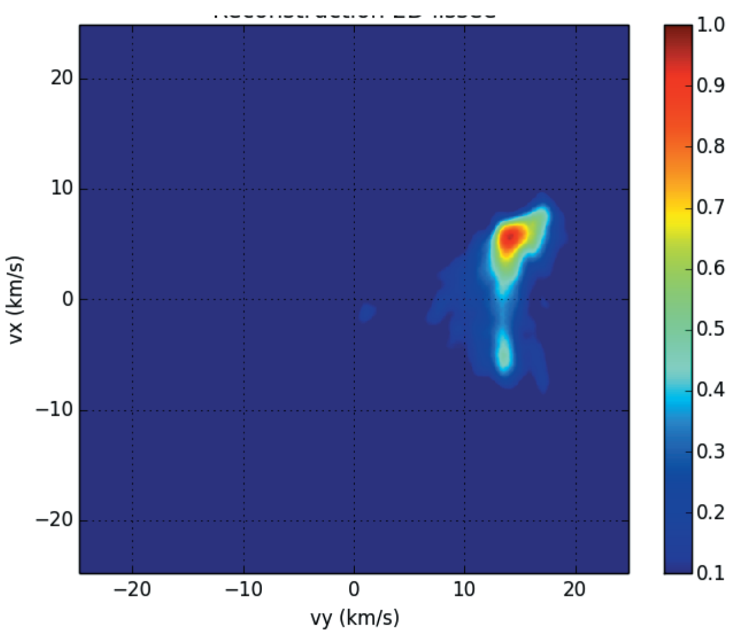

Figure 21- Reconstructed 2D IVDF, case A (in front of the nose cone)

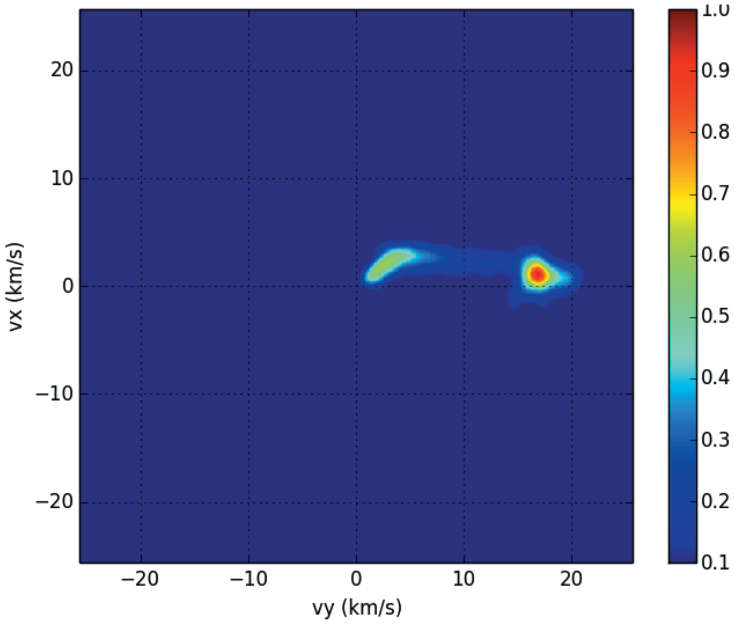

Figure 22- Reconstructed 2D IVDF, case B (in front of the thruster channel)

V. Conclusions

This work has focused on the development of a non-intrusive LIF tomography technique to reconstruct the full ion velocity distribution function of an ion thruster. The principles of the techniques have been presented, as well as the details of the experimental setup specifically developed for this purpose. First, the setup has been used to measure the ion axial velocity across the channel of the thruster, showing the extent of the acceleration region, and also the existence of a cathode-directed velocity in the thruster channel. Second, the tomography has been employed to measure the 2D IVDF in front of the thruster nose cone and the channel. These 2D (in the phase space) reconstructions suggest that the IVDF in front of the thruster nose cone has a toroidal shape. In front of the channel, a fast and a slow ion population are identified.

The extension of this technique to a 3D reconstruction has been explained, and is straightforward with the present experimental arrangement. This will be the object of the next studies.

Acknowledgments

This work is funded under the ESA contract 4000107483/13/NL/SFe. The authors are grateful to Maksym Titov, Maria Smirnova and Pr. Davar Feili for their support during the experiment preparation and the installation of the thruster.

References

1. Cedolin, R. J., Hargus Jr., W. A., Storm, P. V, Hanson, R. K. & Cappelli, M. Laser-Induced Fluorescence Study of a Xenon Hall Thruster. *Appl. Phys. B Lasers Opt.* **65,** 459–469 (1997).
2. Dorval, N. *et al.* Determination of the Ionization and Acceleration Zones in a Stationary Plasma Thruster by Optical Spectroscopy Study: Experiments and Model. *J. Appl. Phys.* **91,** 4811–4817 (2002).
3. Hargus Jr., W. A. & Cappelli, M. Laser-Induced Fluorescence Measurements of Velocity within a Hall Discharge. *Appl. Phys. B Lasers Opt.* **72,** 961–969 (2001).
4. Mazouffre, S., Gawron, D. & Sadeghi, N. A Time-Resolved laser induced fluorescence study on the ion velocity distribution function in a Hall thruster after a fast current disruption. *Phys. Plasmas* **16,** 43504 (2009).

5. Elias, P.-Q. *et al.* Optical Measurements of Neutral Cesium Mass Flow Rate in Field Emission Thrusters. *J. Propul. Power* **27,** 448–460 (2011).
6. McWilliams, R. & Koslover, R. Laboratory observation of ion conics by velocity-space tomography of a plasma. *Phys. Rev. Lett.* **58,** 37–40 (1987).
7. Zintl, M. & McWilliams, R. Improved optical tomography device. *Rev. Sci. Instrum.* **65,** 2574 (1994).
8. Smith, T. B., Herman, D. A., Gallimore, A. D. & Jr, G. J. W. Laser-induced Fluorescence Velocimetry of Xe II in the 30-cm NSTAR-type Ion Engine Plume. *40Th AIAA/ASME/SAE/ASEE Jt. Propuls. Conf.* (2004).
9. Mazouffre, S. Laser-induced fluorescence diagnostics of the cross-field discharge of Hall thrusters. *Plasma Sources Sci. Technol.* **22,** 013001 (2013).
10. Markoe, A. *Analytic Tomography*. (Cambridge University Press, 2006). doi:10.1017/CBO9780511530012
11. Bourgeois, G., Mazouffre, S. & Sadeghi, N. Unexpected transverse velocity component of Xe+ ions near the exit plane of a Hall thruster. *Phys. Plasmas* **17,** 1–6 (2010).